Coupled erosion, climate, and vegetation drove post-MPT maxima in Asian dust activity

Wenxiao Ning,[1,2,3] Jinbo Zan,[1,2,*] Christian Zeeden,[3] Xiaomin Fang,[1,2] Weilin Zhang,[1,2] Yanguang Zhang,[1,2] and Zhe Hu[1,2]

*Correspondence: zanjb@itpcas.ac.cn

Received: November 23, 2025; Accepted: June 8, 2026; Published Online: June 11, 2026; https://doi.org/10.59717/j.xinn-geo.2026.100239

GRAPHICAL ABSTRACT

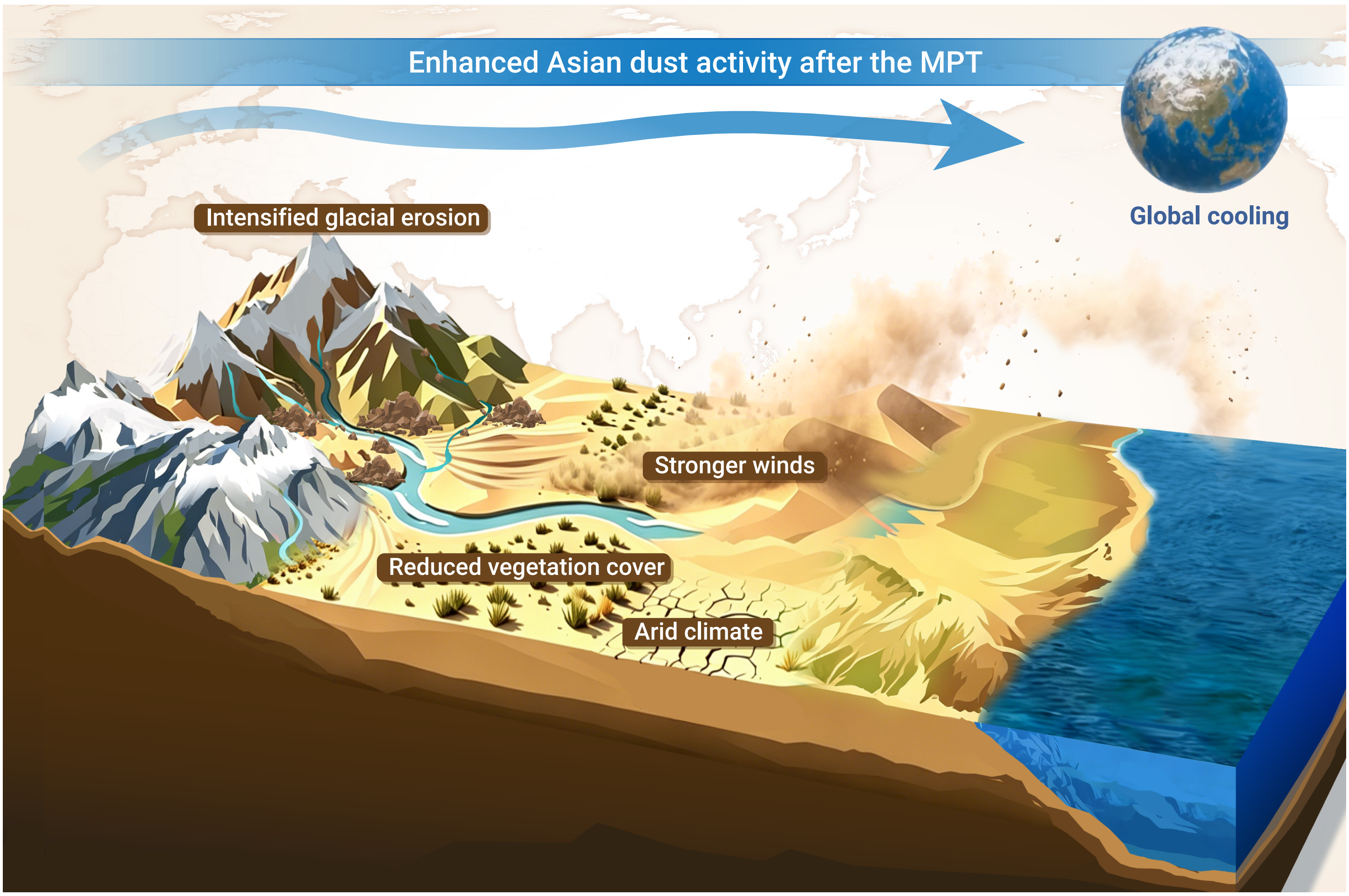

PUBLIC SUMMARY

- Central Asia showed enhanced aridification after ~0.8 Ma, with periodicity shifting from 41 kyr to 100 kyr.
- Asian dust emissions and transport peaked after ~1.0–0.8 Ma, with enhanced glacial–interglacial variability.
- Global cooling drove Asian dust activity by influencing erosion, climate, and vegetation.

Coupled erosion, climate, and vegetation drove post-MPT maxima in Asian dust activity

Wenxiao Ning,[1,2,3] Jinbo Zan,[1,2,*] Christian Zeeden,[3] Xiaomin Fang,[1,2] Weilin Zhang,[1,2] Yanguang Zhang,[1,2] and Zhe Hu[1,2]

[1]State Key Laboratory of Tibetan Plateau Earth System and Resources Environment, Institute of Tibetan Plateau Research, CAS, Beijing 100101, China

[2]University of Chinese Academy of Sciences, Beijing 100049, China

[3]LIAG-Institute for Applied Geophysics, Hannover 30655, Germany

*Correspondence: zanjb@itpcas.ac.cn

Received: November 23, 2025; Accepted: June 8, 2026; Published Online: June 11, 2026; https://doi.org/10.59717/j.xinn-geo.2026.100239

Citation: Ning W., Zan J., Zeeden C., et al. (2026). Coupled erosion, climate, and vegetation drove post-MPT maxima in Asian dust activity. *The Innovation Geoscience* **4**:100239.

The mid-latitude Asian regions are the world's second-largest dust source and are sensitive to global climate change. However, the paucity of inland dust records limits our understanding of regional atmospheric circulation, Asian aridification, and the global climatic and ecological impacts of dust emissions. Here, we present the first high-resolution dust flux record from the arid regions of Central Asia, west of the Pamir Plateau, covering the past 2.7 Myr. By integrating this new record with a compilation of existing datasets, we show that enhanced aridification occurred in Central Asia after ~0.8 Ma, with a dominant periodicity shift from 41-kyr to 100-kyr during the Mid-Pleistocene Transition (MPT). Further, a source-to-sink spatial comparison of dust fluxes indicates that Asian dust activity reached its highest levels after the MPT, accompanied by increased amplitude of glacial–interglacial fluctuations. These patterns correspond strongly with variations in global ice volume across the time–frequency domains, implying a strong coupling between Asian dust activity and global cooling. We propose that, in addition to an arid climate, intensified glacial erosion, and reduced vegetation cover are critical drivers of enhanced Asian dust emissions and transport during periods of global cooling. Under ongoing and projected future global warming, the rapid glacier retreat across the Tibetan Plateau and surrounding mountains, along with regionally increased precipitation and enhanced vegetation cover in dust source regions, may reduce the availability of fine-grained, erodible sediments and stabilize surface soils, gradually weakening Asian dust emissions and their influence on marine productivity and biodiversity in downwind oceans.

INTRODUCTION

The Asian inland arid region, the largest continuous arid zone in the mid-latitudes of the Northern Hemisphere, covers ~7 million km^2 and supports a human population of ~600 million. Characterized by extremely low precipitation, strong evaporation, sparse vegetation cover, and frequent high-intensity winds, this region is prone to severe sandstorm activity and possesses a fragile ecological environment. As the world's second-largest dust source, the mid-latitude Asian arid region emits on average ~2,000 teragrams (Tg; 1 Tg = 10^{12} grams) of dust annually, accounting for nearly 40% of global dust emissions (Figure 1).[1]

On the one hand, fine-grained Asian dust particles are entrained into the upper-level westerlies and transported over long distances to the North Pacific Ocean, the western coast of North America, and Greenland.[2–4] By regulating the Earth's radiative energy balance and influencing marine and terrestrial biogeochemical cycles, these particles profoundly impact regional and global climate systems.[1,5–9] On the other hand, coarse dust particles are predominantly transported by the lower-level westerlies and East Asian winter monsoon (EAWM) to areas downwind of the source deserts, where they accumulate to form red clay and loess–paleosol deposits.[3,10] These eolian deposits record Asian monsoon evolution, westerly circulation dynamics, and Asian inland aridification over millions of years.[11–16] Therefore, elucidating past dust activity in the mid-latitude Asian arid regions is essential for improving our understanding of their future evolutionary trends and the mechanisms linking dust emissions to global climate change. Furthermore, such knowledge provides a critical scientific basis for addressing climate-related challenges and for developing effective strategies to mitigate the environmental impacts of dust emissions in mid-latitude Asia.

To date, records of dust activity from the Asian interior remain scarce, creating a critical knowledge gap that hinders our ability to understand the long-term evolutionary patterns of deserts (e.g., their initial formation timing and expansion phases), as well as the detailed processes of dust release and their relationship with Tibetan Plateau (TP) uplift and global cooling. The few dust flux records currently available are mainly from the Asian monsoon-influenced Chinese Loess Plateau (CLP) and the central-southern margin of the Tarim Basin on the leeward side of the westerlies.[14,17–19] Although several geochronological studies based on desert boreholes and adjacent loess deposits have yielded preliminary insights into the initial formation time of deserts,[12,15,20–25] these records cannot provide detailed and continuous records of dust emission across the Asian interior. An additional major limitation is the lack of spatially integrated, multi-proxy source-to-sink comparisons between Asian inland eolian systems and North Pacific sedimentary archives. Previous comparisons of dust flux records between the CLP and North Pacific sediment cores have largely emphasized long-term trends;[18,26–28] however, they are typically based on isolated site pairs and lack a coordinated, hemispheric-scale synthesis. This deficiency not only hinders the refinement of predictive models for future dust activity but also limits our understanding of Asian dust's role in global biogeochemical cycles and climate feedback mechanisms.

Eolian loess deposits are widely distributed in Tajikistan, with thicknesses locally exceeding 200 m (Figure 2).[29,30] A recent magnetostratigraphic study revealed that the Karamaidan (KMD) loess section in southern Tajikistan extends back to ~2.7 Ma,[31] providing a novel and continuous archive for investigating dust emission processes in typical westerlies-dominated regions since the late Pliocene. In this study, we present the first high-resolution dust flux record from the arid region of Central Asia west of the Pamir Plateau, spanning the past 2.7 Myr, and conduct a comprehensive source-to-sink spatial comparison between the Asian interior and North Pacific dust fluxes. Based on these results, we propose a mechanistic framework for Asian dust dynamics: Northern Hemisphere ice volume expansion facilitated dust emissions and transport in the Asian interior via concurrent enhanced glacial erosion, climatic aridity, strengthened winds, and reduced vegetation cover.

MATERIALS AND METHODS

Tajikistan preserves the most continuous and oldest loess–paleosol sequence in western Central Asia. Recent magnetostratigraphic investigations constrain the basal age of the Karamaidan (KMD) section in southern Tajikistan to ~2.7 Ma.[31] The KMD section exposed at the site is ~180 m thick and spans 2.7–0 Ma; however, a ~15 m interval (1.65–1.37 Ma) is unsampled due to poor exposure. These eolian deposits are characterized by reddish-yellow loess layers and reddish-brown paleosol layers, which formed during glacial and interglacial periods, respectively. The lithological features closely resemble those of the Chashmanigar section in Tajikistan, and the CLP loess–paleosol sequences (Figure 3).[29,35] The entire 180-m-thick KMD loess–paleosol sequence was sampled at a ~20 cm resolution, providing an exceptional archive of Central Asian dust activity over the past 2.7 Myr.

The mass accumulation rate (MAR; g·cm^{-2}·kyr^{-1}), also called dust flux, is widely used as an effective proxy for aridity variability in the dust source regions.[14,19] Dust flux is usually obtained by measuring and calculating dry bulk sediment densities and sedimentation rates.[19] Accordingly, the MAR for the KMD section was calculated as

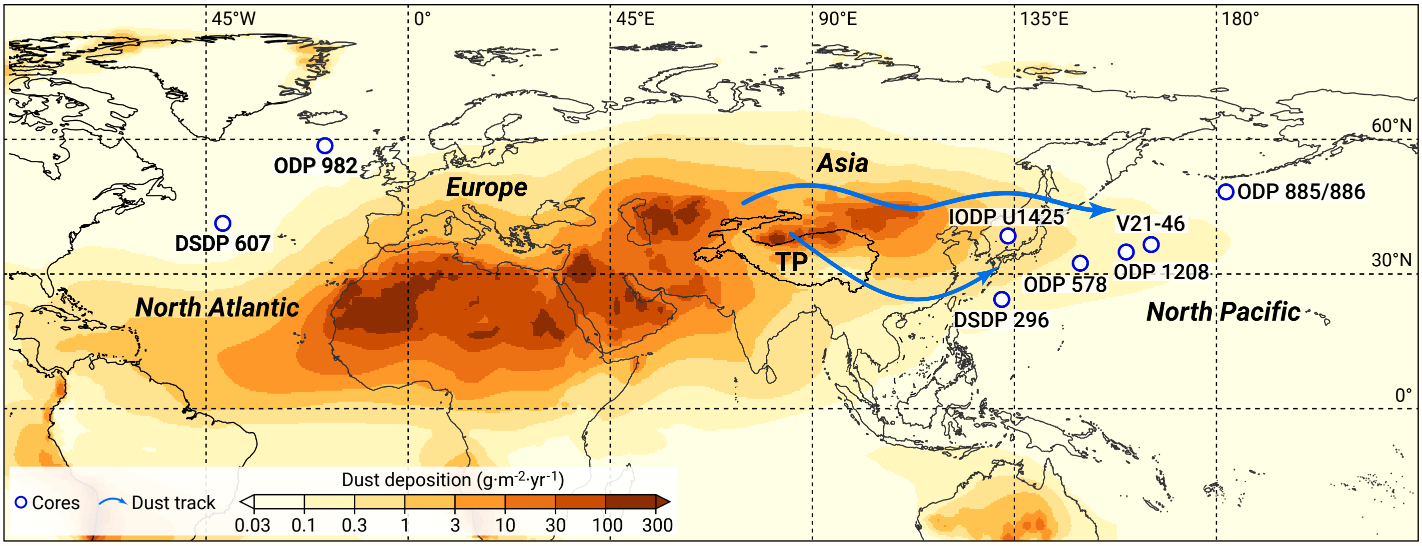

Map Approval Number: GS(2016)1666

Figure 1. Spatial distribution of atmospheric dust deposition across the Eurasian continent for the period 1998–2010 Data are obtained from ref.[32]

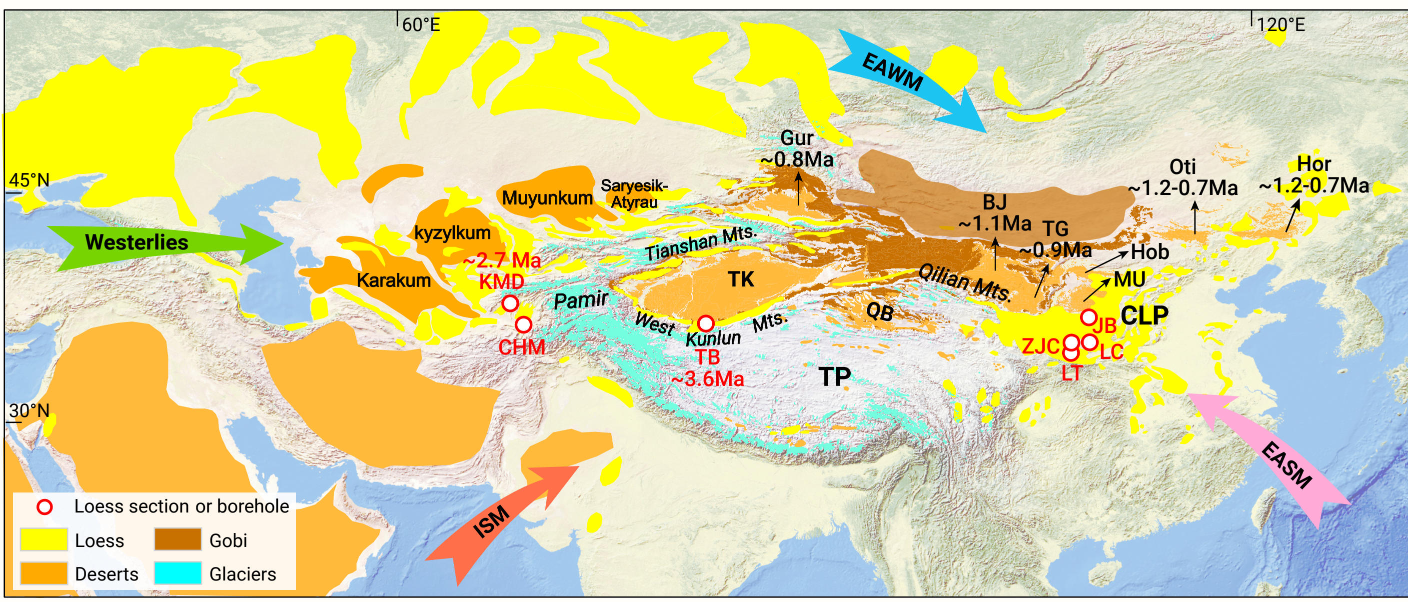

Figure 2. Synthesis of the initiation time and spatial distribution of major deserts and loess deposits in Asia Data on loess, deserts, and glaciers are derived from the Desert Distribution Dataset in China (http://westdc.westgis.ac.cn/), and the Randolph Glacier Inventory v7.0 from NSIDC (https://doi.org/10.5067/f6jmovy5navz).[33,34] TP: Tibetan Plateau. CLP: Chinese Loess Plateau. QB: Qaidam Basin. KMD (this study) and CHM: Karamaidan and Chashmanigar loess sections in southern Tajikistan. TB: The 671 m-loess borehole in the southern Tarim Basin. LT, LC, JB, and ZJC: Lingtai, Luochuan, Jingbian, and Zhaojiachuan red clay and loess–paleosol sections on the CLP. TK, Gur, QB, BJ, TG, MU, Hob, Hor and Oti: Taklimakan, Gurbantunggut, Qaidam Basin, Badain Jaran, Tengger, Mu Us and Hobq deserts, Horqin and Otindag sandy lands in Central and East Asia. Initiation time of deserts and loess deposits are summarized in Table S1. EAWM and EASM: East Asian winter and summer monsoons. ISM: Indian summer monsoon.

$$MAR = f_{eolian} \times SR \times DBD$$

where SR (cm·kyr^{-1}) is the sedimentation rate, and DBD (g·cm^{-3}) is the dry bulk density. Because loess–paleosol and red clay deposits are generally considered to be entirely of eolian origin,[37–39] $f_{eolian} = 1$ is often assumed when estimating dust flux for eolian deposits on the CLP and Central Asia. The SR was calculated through stratigraphic correlation (Figure 3), combined with a magnetic susceptibility age model.[40] Further details are provided in Text S1.

To enable a comprehensive spatial comparison of dust fluxes between terrestrial and marine sediments, published records of dust fluxes from Asian eolian deposits along with those from North Pacific sediment cores were compiled.[14,17,19,27-28,41-46] To further investigate the rhythms, trends, and periodic characteristics of the dust fluxes, we applied statistical analyses, including the Mann–Whitney and Ansari–Bradley tests, and time series analysis. Detailed descriptions of the analytical procedures are provided in Texts S2–S3.

RESULTS AND DISCUSSION

Dust emission history in Central Asia since the late Pliocene

Central Asian dust emissions play a critical role in regulating regional climate dynamics and global biogeochemical cycles.[1,5–9] To elucidate the Central Asian dust emission history, we investigated the loess dust flux, property, and periodicity in southern Tajikistan. We then integrated these new results with previously published loess dust record from the Tarim Basin to constrain the dust emission patterns in Central Asia over geological timescales.

The dust flux record at Karamaidan in southern Tajikistan varied between 1.8 and 60.6 g·cm^{-2}·kyr^{-1}, with a mean of 12.6 g·cm^{-2}·kyr^{-1} (Figures 3 & 4A). Dust flux values in loess units are consistently higher than those in paleosol units (Figures 3 & 4A), indicating more intense dust activity and enhanced dust accumulation during loess deposition compared with periods of paleosol formation. To better characterize the long-term trends of dust flux, we

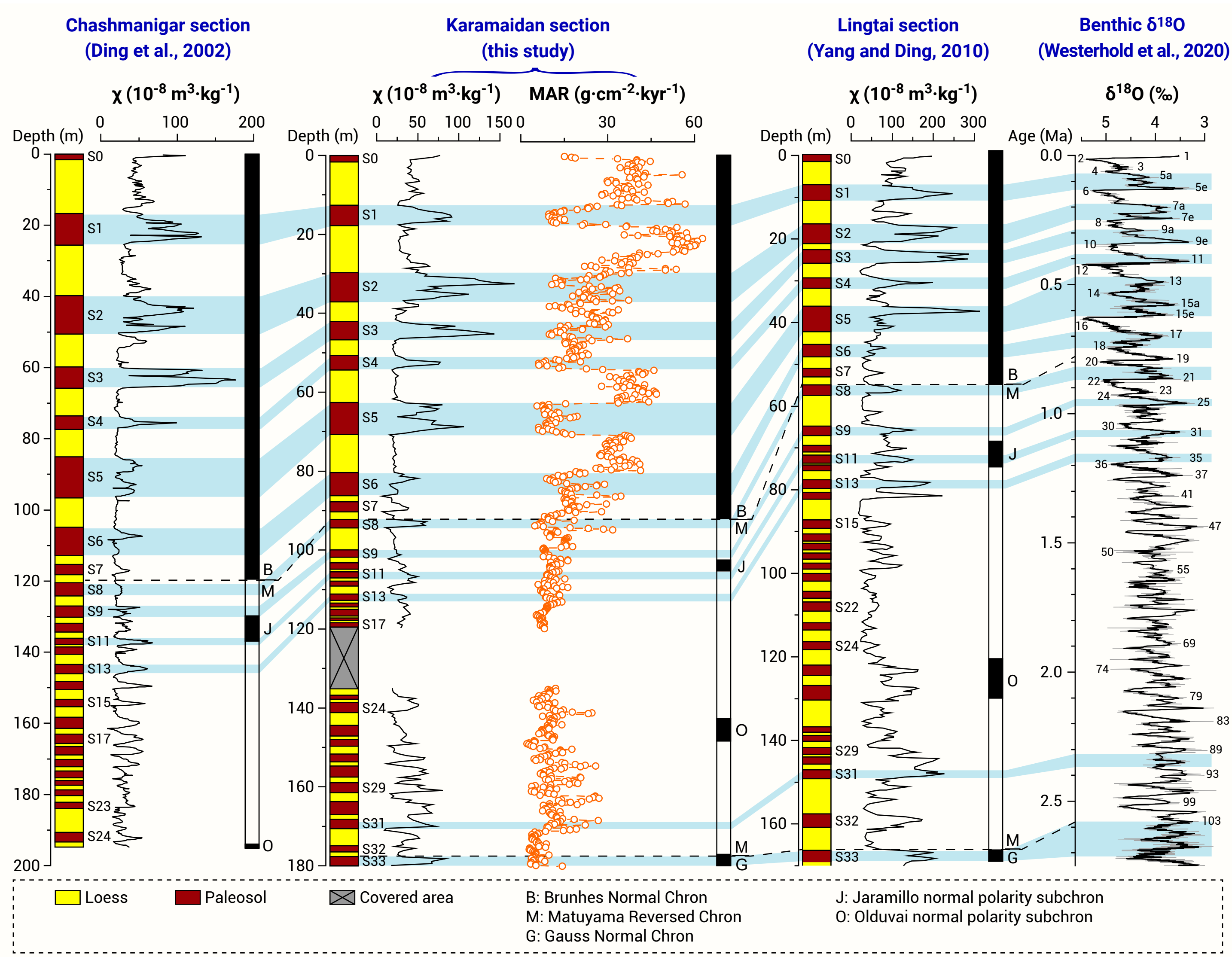

Figure 3. Correlations of lithostratigraphy, magnetostratigraphy, and magnetic susceptibility (χ) records of the Chashmanigar and Karamaidan sections in southern Tajikistan, the Lingtai section on the Chinese Loess Plateau, and the benthic $\delta^{18}O$ stack Data are derived from refs.[29,31,35,36]

applied the Mann–Whitney test to the KMD record. The results reveal a persistent increasing trend (marked by red arrows in Figure 4A) throughout the past 2.7 Myr, spanning both glacial and interglacial intervals, with an acceleration after the Mid-Pleistocene Transition (MPT; ~1.25–0.7 Ma). When loess and paleosol layers are analyzed independently, the upward trend in dust flux becomes even more pronounced, highlighting the systematic intensification of dust accumulation through time. Given that the Tajikistan loess is dominantly sourced from dust transported by the westerlies from upwind Central Asian deserts, with only a minor contribution from proximal alluvial deposits in the adjacent mountains and fluvial/glaciofluvial sediments on river floodplains,[47,48] this long-term increase in loess dust flux implies the substantial enhancement of dust emissions from Central Asian deserts (e.g., the Karakum and/or Kyzylkum deserts), particularly after the MPT.

In addition to the long-term trends in dust flux, we also assessed fluctuations in dust flux using the Ansari–Bradley test, a nonparametric statistical approach that quantifies differences in data dispersion. The results demonstrate that the amplitude of dust flux fluctuations on glacial–interglacial timescales increased significantly after the MPT (denoted by blue arrows in Figure 4A), indicating an enhanced climate-driven dust flux variability in response to the post-MPT reorganization of the global climate system. To examine the role of orbital forcing on dust flux variations, we conducted spectral analysis of different time intervals (Figure 4C). Before the MPT (2.7–0.8 Ma), dust flux was dominated by a 41-kyr periodicity, consistent with the obliquity cycle; after the MPT (0.8–0 Ma), dust flux exhibits a prominent 100-kyr periodicity, corresponding to the eccentricity cycle and glacial/interglacial cycles (Figures 4C–D). This shift in dominant periodicity aligns closely with global ice volume variability inferred from a benthic $\delta^{18}O$ stack,[49] suggesting that Central Asian dust dynamics were tightly coupled to global ice volume changes since the late Cenozoic.

Concurrent with the Tajikistan loess record, loess dust flux from the southern margin of the Tarim Basin increased from 12–20 $g \cdot cm^{-2} \cdot kyr^{-1}$ before the MPT to 20–30 $g \cdot cm^{-2} \cdot kyr^{-1}$ after the MPT,[14] also providing strong evidence for enhanced post-MPT dust emissions across Central Asia (marked by red arrows in Figure 4E). Spectral analysis of the > 30 μm grain-size record from Tarim Basin loess further reveals a clear periodicity transition at the MPT, from 41-kyr to 100-kyr,[14] in agreement with global ice volume (Figures 4H–I).[49]

The lithogenic susceptibility (χ_{litho}) of eolian loess can reflect dust properties and material compositions.[50–53] In Central Asian loess, χ_{litho} exhibits a trend broadly consistent with variations in dust flux (Figure 4B),[51] indicating that a large amount of fresh and unaltered detritus rich in detrital magnetite particles, likely from the Tianshan–Pamir, was added to Central Asian dust and subjected to weak low-temperature oxidation and limited chemical weathering after the MPT. Chlorite, a common Fe^{2+}-bearing silicate mineral in Asian eolian loess, is a sensitive tracer for dust source lithology. Both the

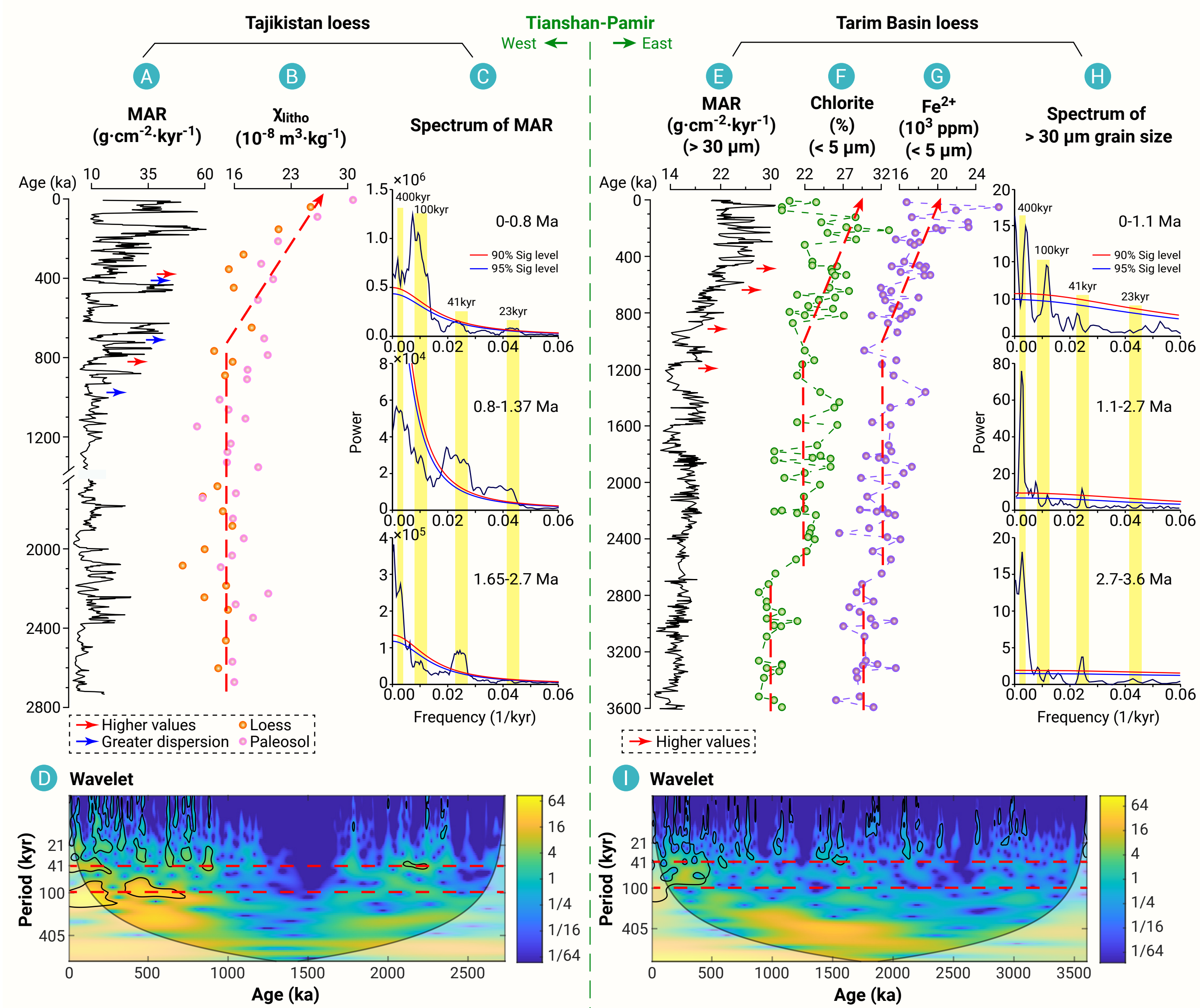

Figure 4. **Comparison of dust fluxes, properties, and periodicities between Tajikistan and Tarim Basin loess records** (A–D) Tajikistan loess. (E–I) Tarim Basin loess. The red and blue arrows in (A) and (E) show the breakpoints of the increased central tendency and dispersion of dust fluxes determined by the Mann–Whitney and Ansari–Bradley tests, respectively (Figure S1). Note that dust fluxes increased significantly after the Mid-Pleistocene climate transition (MPT) on both the windward and leeward sides of the westerlies. The bold red dashed lines in (B), (F), and (G) denote the increasing trends of lithogenic susceptibility, chlorite, and Fe^{2+}, which are indicators of dust properties. χ_{litho}, chlorite, and Fe^{2+} further indicate that more fresh and unaltered detritus was added to Central Asian dust after the MPT. Spectral (C and H) and wavelet (D and I) analyses reveal analogous periodicity patterns, characterized by a dominant 41-kyr cyclicity prior to the MPT and a shift to a dominant 100-kyr cyclicity post-MPT. Data on the χ_{litho} of Tajikistan loess, dust flux, Fe^{2+}, chlorite, and spectral analysis results for the Tarim Basin loess are derived from refs.[8,14,51,54]

chlorite content and Fe^{2+} concentration in Tarim Basin loess show marked increases at the MPT, with chlorite rising from ~17%–26% to ~21%–32% and Fe^{2+} from ~9,000–16,000 ppm to ~14,000–24,000 ppm (Figures 4F & G).[8,54] In concert with the enhanced dust flux, these geochemical shifts confirm the increased supply of fresh and unaltered clastic sediments from the northern TP to the Tarim Basin dust after the MPT. Combining the above observations shows that loess dust fluxes, properties, and periodicities are coupled across both the windward side (e.g., southern Tajikistan) and leeward side (e.g., southern Tarim Basin) of the westerlies.

Spatiotemporal dynamics of Asian dust activity during the Plio–Pleistocene

Our results demonstrate that loess dust fluxes in southern Tajikistan display a long-term increasing trend since ~0.8 Ma (Figure 5A), suggesting that Central Asian deserts, such as the Karakum and/or Kyzylkum, may have expanded after the MPT. In the southern margin of the Tarim Basin, the coarse grain size fraction (> 30 μm) and the related loess dust flux exhibit stepwise increases at ~2.7, 1.1, and 0.5 Ma, suggesting the stepwise aridification of Central Asia and progressive expansion of the Taklimakan Desert (Figure 5B).[14] To further understand the spatiotemporal variations of dust emissions across Asian dust source regions, we compared the dust records from northern China over the same interval. On the southern CLP, dust flux records from the Lingtai, Zhaojiachuan, and Luochuan sections show large-amplitude, high-frequency variability since ~1.2–0.8 Ma (Figures 5C–E),[17–19] indicating that the dust activity of the Gobi, Badain Jaran, and Tengger deserts northwest of the CLP intensified after the MPT.

However, loess dust fluxes in Central Asia, which are closer to major dust sources such as the Taklimakan and Karakum deserts, are consistently higher and show greater glacial–interglacial variability than those on the CLP, indicating a stronger response to regional aridification and dust emission dynamics (Figures 5A & C–E). This contrast is likely governed by at least two factors: differences in the transport distance between dust source and deposition regions, and the contrasting environmental and climatic conditions

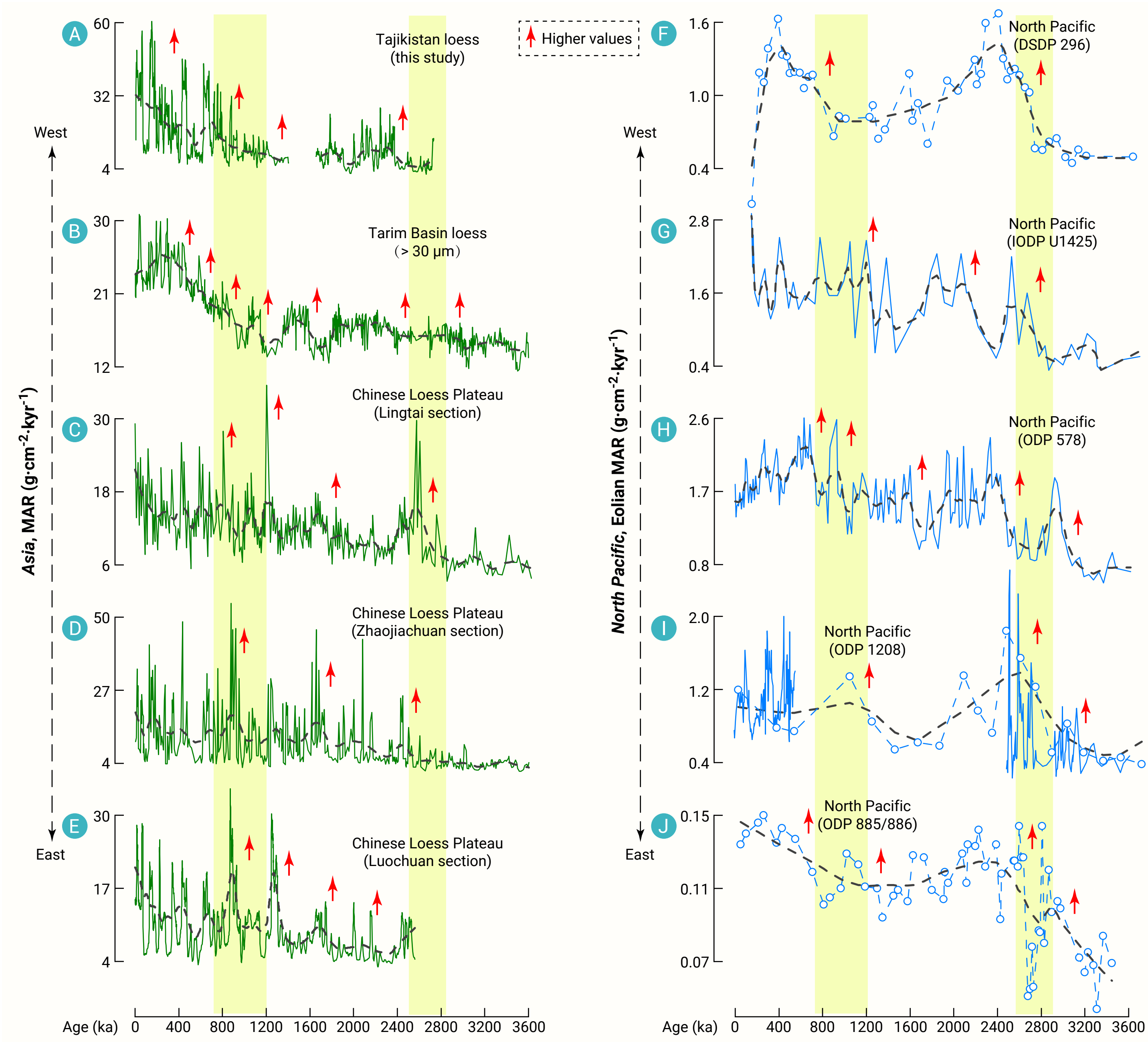

Figure 5. Temporal and spatial variations of eolian dust fluxes in Asia and the North Pacific over the past 3.6 Myr (A–E) Asian dust flux records. (F–J) North Pacific eolian dust flux records. Dust fluxes are derived from this study and refs.[14,17,19,27–28,41–43,45–46] The geographic locations of all sites are shown in Figures 1–2. The black dashed lines in each dust flux plot are locally weighted scatterplot smoothing (LOWESS) using 250 kyr (A–E, G and H) and 1000 kyr (F, I and J) windows. The red arrows show the breakpoints of increased dust fluxes determined by the Mann–Whitney test (Figure S1). The yellow bands represent the Mid-Pleistocene climatic transition and 2.8–2.6 Ma.

during glacial and interglacial periods. Although hydroclimatic conditions on the western and eastern sides of the Pamir–Tianshan region exhibit contrasting seasonal patterns since at least ~25 Ma,[55] long-term dust flux records from both regions show broadly coherent trends during the late Pliocene–Pleistocene, differing mainly in the magnitude and amplitude of glacial–interglacial fluctuations.

In addition, independent evidence from geochronological data and coarse-fraction records from deserts and adjacent eolian or lacustrine deposits further supports our conclusions (Table S1). In the Qaidam Basin, a long-term upward coarsening trend of grain size of lacustrine sediments implies enhanced eolian inputs at ~1.1 Ma.[56] In the Central CLP, the continuous increase in the sand content (> 63 μm) of the Jingbian loess sequence suggests the southward migration of the Mu Us Desert at ~2.6 and 1.2–0.7 Ma.[15] The lithologies of the Badain Jaran and Tengger deserts changed abruptly from alluvial/fluvial sediments to continuously accumulated eolian sand at ~1.1 Ma and ~0.9 Ma, respectively.[21,22] These lithological transitions provide direct evidence for intensified dust activity in both deserts following the MPT. The presence of eolian sand in the basal section of the core from the central Hetao Basin suggests that eolian activity linked to the Hobq Desert was already underway by ~1.6–1.2 Ma.[20] In some Asian inland dust source regions, where continuous desert sediment drilling cores are scarce, the onset of proximal eolian loess deposition offers a valuable minimum constraint on the timing of sustained dust activity. For instance, the initiation of loess deposition in profiles surrounding these source areas indicates that the Gurbantunggut Desert, as well as the Horqin and Otindag sandy lands, were likely established during ~1.2–0.7 Ma.[57–59]

The North Pacific Ocean is a major sink for long-distance-transported dust from Asian deserts, and dust flux records from this region provide critical insights into the history of Asian dust emission and transport. To better understand long-range dust transport since the late Pliocene, we compiled

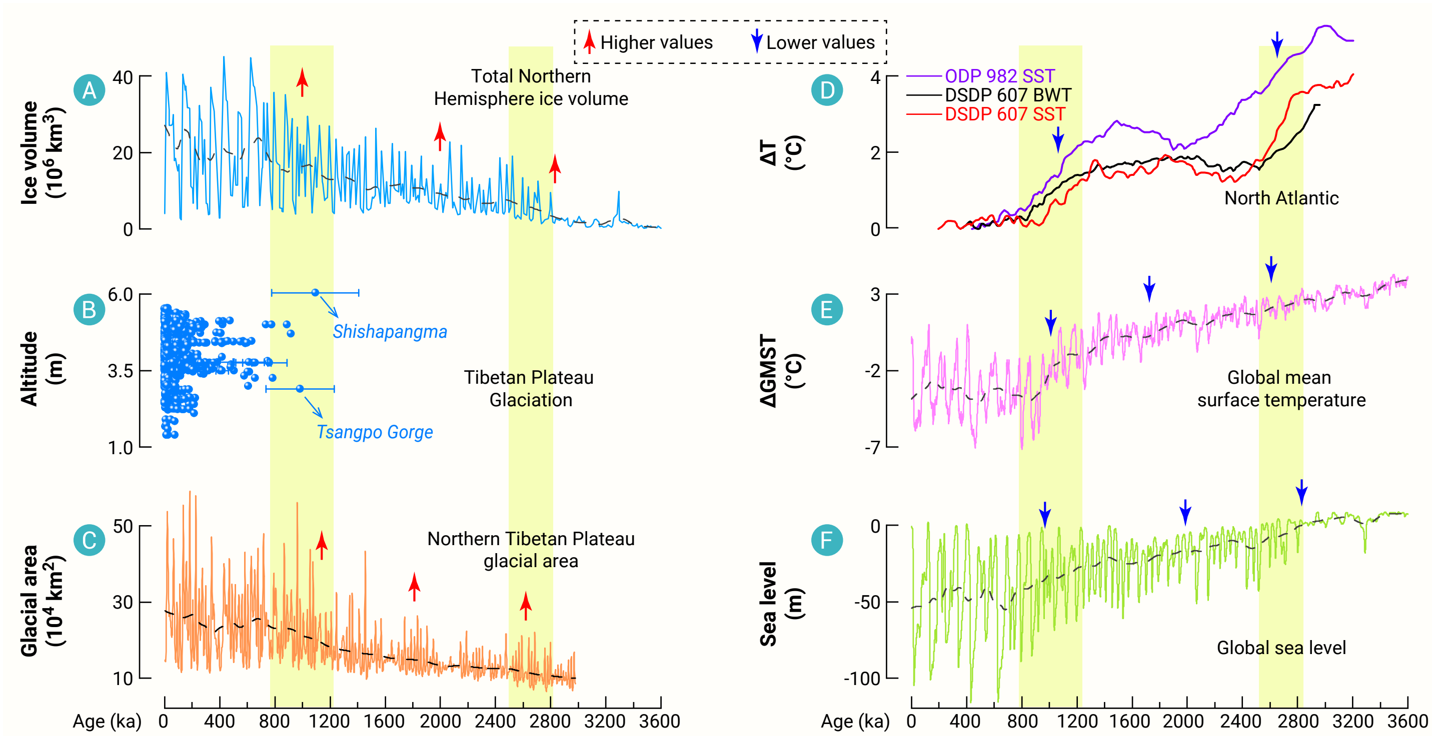

Figure 6. Temporal variations of various paleoclimate proxies over the past 3.6 Myr (A) Total Northern Hemisphere ice volume.[102] (B) Synthesized ages of paleoglaciation on the Tibetan Plateau (TP).[85–89] (C) Glacier area evolution on the northern TP encompasses the Pamir, Tianshan, and Qilian Mountains, and adjacent regions.[90] (D) Sea surface temperature (SST) and bottom water temperature (BWT) variations from ODP 982 and DSDP 607 in the North Atlantic.[91] (E) Changes in global mean surface temperature.[103] (F) Eustatic sea level.[102] The black dashed lines in (A, C, E–F) are locally weighted scatterplot smoothing (LOWESS) using 250 kyr windows. The red and blue arrows (A, C–F) show the breakpoints of increased/decreased trends determined by the Mann–Whitney test (Figure S4). The yellow bands represent the Mid-Pleistocene climate transition (MPT) and 2.8–2.6 Ma.

published eolian dust flux records from multiple sites in the North Pacific. These include Deep Sea Drilling Project (DSDP) Site 296; Ocean Drilling Program (ODP) Sites 885/886, 578, and 1,208; and International Ocean Discovery Program (IODP) Site U1425, all situated within the primary downwind deposition zone of Asian dust and thus preserving robust archives of eolian input to the North Pacific over the past ~3.6 Myr. Eolian dust fluxes from several of these sites exhibit consistent increasing trends at 2.8–2.6 Ma and at the MPT (Figures 5F–J),[27-28,41-43] indicating intensified dust emissions and enhanced atmospheric transport from Asian source regions at these times.

Spatially, eolian dust fluxes at ODP Sites 885/886 in the central North Pacific range from ~0.04 to 0.15 g·cm^{-2}·kyr^{-1} (Figure 5J),[28] which is an order of magnitude lower than values recorded in the western North Pacific (Figures 5G–I). In the western North Pacific, dust fluxes systematically decreased with increasing distance from the Asian dust source regions, reflecting progressive dilution and depositional loss during long-distance atmospheric transport (Figures 5G–I).[41,44,60-61] At DSDP 296, the relatively low dust flux is likely related to its location outside the main mid-latitude westerly dust-transport corridor (Figure 5F).[42] In addition, both Asian inland and North Pacific dust fluxes display glacial–interglacial variability, with higher dust fluxes during glacials and lower values during interglacials (Figure S2).[44,62]

The source-to-sink spatial comparison of dust fluxes indicates that Asian dust activity reached its highest levels after the MPT, accompanied by an increase in the amplitude of glacial–interglacial fluctuations. Prior to the MPT, dust activity in Asian deserts was relatively weak, and loess dust accumulation was largely confined to Central Asia and the CLP. In contrast, after the MPT, Asian desert dust activity intensified markedly, accompanied by widespread and enhanced loess accumulation in northern China. Notably, the dominant periodicity of high-resolution loess dust fluxes shifted from 41-kyr to 100-kyr at the MPT, a transition also evident in records from the CLP and Central Asia.[14,17] These features align closely with global ice volume changes in the time and frequency domains, highlighting that global cooling may have driven enhanced Asian dust emission, transport, and accumulation after the MPT.

Global cooling drove the increasing emission and transport of Asian dust after the MPT

The formation of eolian deposits generally comprises particle generation, erosion, transportation, and accumulation.[63–65] The primary source materials for Asian dust are largely derived from sediments produced by glaciers on the Tibetan Plateau and its surrounding mountain ranges.[3,64,66] These glaciogenic sediments are subsequently transported via river systems into inland basins, where they undergo eolian sorting and accumulation to form desert landscapes under dry conditions.[3,64,66] Once wind-entrained, these desert-derived sediments are transported downwind and ultimately deposited as extensive loess–paleosol sequences in the downwind areas of these deserts. Therefore, the release, transport, and accumulation of Asian dust depend on several fundamental prerequisites, including adequate sand source availability, arid to semi-arid climatic conditions, vigorous wind systems, and an open underlying surface environment.

Our synthesis of integrated datasets reveals a marked increase in dust emissions from Asian deserts between 1.2 and 0.7 Ma, broadly coincident with the global cooling associated with the MPT (Figure 5). Cross-wavelet transform and wavelet coherence analyses between Asian dust fluxes and global ice volume show that the two series exhibit resonant high-energy signals at a 41-kyr cyclicity prior to the MPT, and 100-kyr cyclicity thereafter (Figures S3A–C). These observations highlight the strong control of global cooling on Asian dust emissions. Post-MPT global cooling drove large-scale expansions of the Cordilleran, Laurentide, and Greenland ice sheets in North America, as well as the Scandinavian, British–Irish, and Kara–Barents Sea–Svalbard ice sheets in Northern Europe, and Nordic sea ice (Figure 6A).[67–75]

The large-scale expansion of Northern Hemisphere ice sheets exerted three primary controls on Asian dust dynamics. First, intensified glacial conditions enhanced glacial erosion or river incision in the mountains surrounding the dust source regions, thereby generating abundant detrital materials and supplying sufficient sediments available for dust emissions.[66,76–82] Second, increased ice volume intensified aridity across Asia while simultaneously strengthening the westerlies and EAWM, a combination

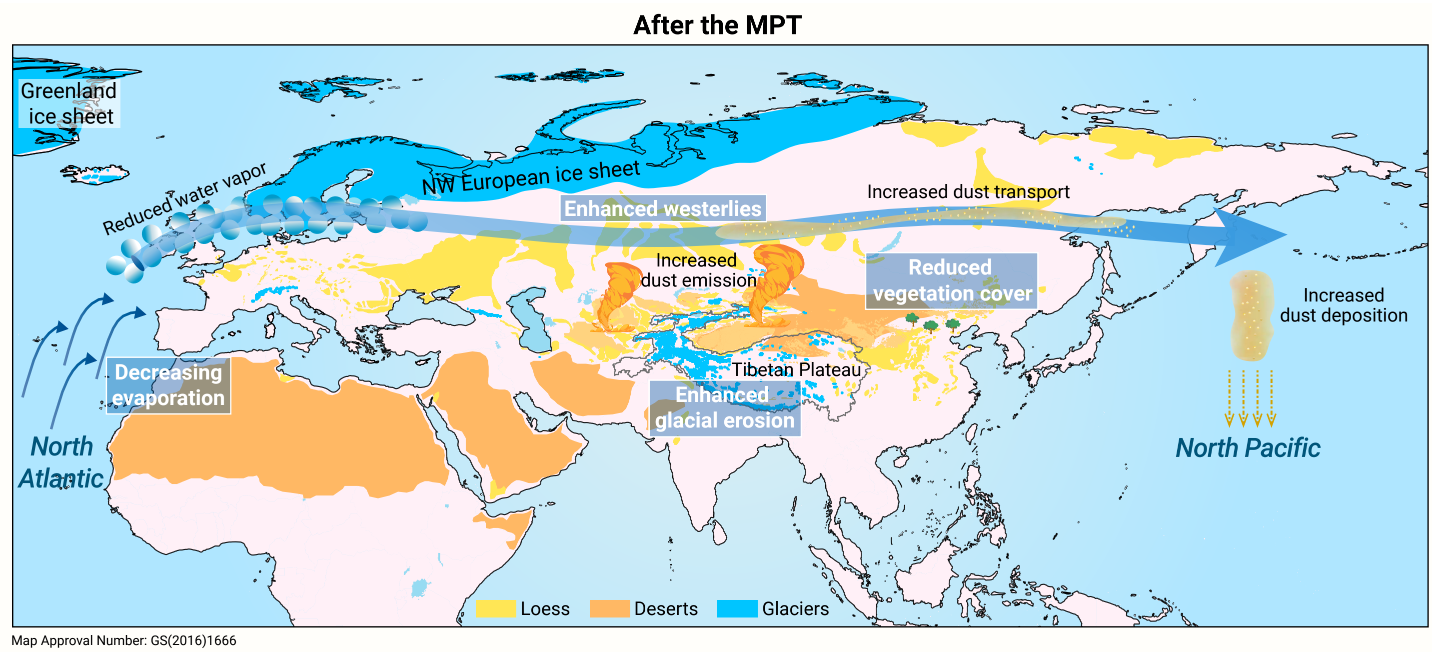

Figure 7. Conceptual model of the driving mechanisms of dust emission and transport in the Asian interior during geological intervals of global cooling Data on loess, deserts, and glaciers are derived from refs.[33,34], the Desert Distribution Dataset in China (http://westdc.westgis.ac.cn/), and the Randolph Glacier Inventory v7.0 from NSIDC (https://doi.org/10.5067/f6jmovy5navz). Ice sheets are drawn based on refs.[67–74]

that facilitated dust emissions and long-distance dust transport.[14,15] Third, the shift toward colder and drier climates drove a large-scale ecological transition from forest to woodland and steppe landscapes, producing more open, sparsely vegetated surfaces that are optimal for dust emissions and transport.[14,83,84]

Previous studies have demonstrated that the growth of Northern Hemisphere ice sheets during the MPT intensified physical weathering and glacial erosion in the mountainous regions surrounding Asian dust source areas.[80–82] This enhanced erosion generated substantial amounts of rock debris, resulting in an abundant and continuous sediment supply for deserts and eolian deposits. Concurrently, the shift in climate variability from relatively stable conditions to large-amplitude, high-frequency fluctuations strengthened river incision, producing additional sediments that accumulated in exposed valleys and further sustained the sediment supply to deserts and eolian loess.[77–79,82] Multiple dust-related proxies from Asian loess, including lithogenic susceptibility, chlorite, and Fe^{2+}, are closely related to the physical erosion intensity of continental glaciers.[8,50–52,54] The marked increase in these proxies after ~0.8 Ma suggests a significant intensification of physical erosion in the TP following the MPT, producing large amounts of sand sediments required for Asian deserts and eolian deposits. Consistently, synthesized ages from glacial deposits indicate that moraines became widespread on the TP after the MPT,[85–89] pointing to the significantly enhanced paleoglaciation (Figure 6B). Recent numerical simulations further reveal that intensified TP glaciation occurred at ~1.5 Ma, and stabilized into a 100-kyr cyclicity at ~1.0–0.9 Ma (Figure 6C),[90] broadly coeval with the increased trend and amplitude of Asian dust fluxes. This synchronicity implies that the expansion of ice caps and valley glaciers boosted detrital sediment production, ultimately providing sufficient sand sediments for Asian deserts and loess deposits.

The intensified glacial conditions during the MPT lowered sea temperatures (Figures 6D– E) and sea level (Figure 6F), and weakened oceanic evaporation, resulting in a substantial decrease in moisture supply and the further enhancement of aridification in the Asian interior. Cross-wavelet and coherence analyses show that North Atlantic sea surface temperatures and global ice volume exhibit resonant, high-energy 41-kyr and 100-kyr cyclicities,[91] consistent with the spectral relationships between Asian dust fluxes and global ice volume (Figure S3). Such coherence suggests the tight coupling among Northern Hemisphere ice volume, North Atlantic temperatures, and Asian dust fluxes. Geological evidence shows that the modern landscape of the Taklimakan Desert was established at ~0.7–0.5 Ma, coincident with the late Mid-Pleistocene climatic reorganization.[14,83] Deserts across northern China, including the Gurbantunggut, Badain Jaran, Tengger, Mu Us, and Hobq deserts, as well as the Horqin and Otindag sandy lands, were primarily established and expanded during the MPT (Figure 2 & Table S1).[15,20-22,57-59] The widespread expansion of these desert systems effectively shortened the distance and time required for dust transport from source to depositional areas, thereby enhancing post-MPT dust emission.

In addition, the growth of Northern Hemisphere ice sheets intensified the EAWM and westerly circulation, providing the dynamic conditions necessary for long-distance dust transport. Grain size data from Central Asian loess sequences and North Pacific cores are widely used as proxies for mid-latitude westerly wind intensity. The content of coarse grains (> 30 μm) in loess deposits and paleoclimate simulations of the Tarim Basin show that the expansion of the high-latitude ice sheets at ~2.7 Ma and during the MPT greatly increased the wind speed in both the upper-level and near-surface westerlies, thereby promoting increased dust release and transport in eastern Central Asia (Figure S5A).[14] Similarly, pronounced rises in coarse particles (> 63 μm) in the Jingbian loess section on the CLP at ~2.7 and 1.2–0.7 Ma reflect strengthened EAWM, which facilitated the release of desert dust and its subsequent transport to the CLP (Figure S5B).[15] The eolian grain size records from ODP 885A and DSDP 578 show long-term coarsening trends during the Plio–Pleistocene, indicating the gradual intensification of the zonal westerlies that would have enhanced the long-distance transport of Asian dust to the North Pacific (Figures S5C–D).[28,41] All records exhibit a pronounced coarsening of eolian grain size after the MPT, which is commonly interpreted as evidence for a strengthened westerlies and EAWM that facilitated the increased delivery of dust particles.

Vegetation plays a pivotal role in influencing soil and landscape stability and thus is a key regulator of eolian processes. A dense vegetation cover mitigates soil erosion by reducing near-surface wind speeds and suppressing eolian erosion, whereas sparse or degraded vegetation markedly enhances the surface erodibility and facilitates the rapid expansion of eolian deposits across Eurasia. Particularly, the establishment and long-term persistence of grassland ecosystems created open, stable, and low-roughness surface conditions that supported continuous loess accumulation.[84,92] Pollen and carbon isotope records from continental Asia document a profound ecological reorganization during the MPT, characterized by a transition from closed forest or woodland to more open steppe or desert.[93–100] In major dust source areas, particularly the Tarim and Qaidam Basins, the vegetation degraded markedly after ~0.9–0.6 Ma, with the pronounced expansion of xerophytic taxa (e.g., *Chenopodiaceae*, *Artemisia*), signaling a transition from dry steppe to open desert or semi-desert (Figures S6A–B).[83,97] This loss of vegetation cover would have reduced surface stability and greatly enhanced sediment erodibility and dust availability, directly amplifying dust emission intensity from source areas. Concurrently, in the downwind regions of the CLP and northeastern China, pollen assemblages shifted from mixed coniferous–broadleaf forest to herb-dominated steppe or forest-steppe after ~0.7–0.6 Ma (Figures S6C–E).[93-96,98,100] This large-scale grassland expansion not only reflects regional aridification but also improves surface dust-trapping efficiency; the dense herbaceous root systems and low-surface roughness help stabilize deposited dust and sustain persistent loess accumulation. Together, these spatially coherent changes—including reduced vegetation cover in source regions boosting dust supply, and grassland development in sink regions enhancing dust retention—provide robust paleoecological support for an intensified dust cycle in the post-MPT period.

Although the tectonic uplift of the TP may modulate long-term aridification and dust availability in the Asian interior, it operates on fundamentally different timescales than orbital-driven dust variability. Specifically, dust flux records exhibit pronounced glacial–interglacial cyclicity (Figure S2), whereas major tectonic episodes of the TP operate over millions of years and lack orbital-scale periodicities.[55,101] This discrepancy strongly suggests that TP uplift may act as a secondary superimposed factor on Asian dust activity, rather than the primary driver.

This study conducts a comprehensive spatial comparison of eolian dust fluxes between the Asian interior and the North Pacific since the late Pliocene. It offers a novel perspective that enhanced glacial erosion and reduced vegetation cover are additional key drivers of intensified Asian dust emissions during geological intervals of global cooling, complementing the traditional view that dust emissions are governed primarily by arid climatic conditions. We propose a mechanistic framework for Asian dust dynamics whereby Northern Hemisphere ice volume expansion, identified as the primary forcing, promotes dust emissions and transport by concurrently intensifying glacial erosion, aridity, winds, and vegetation loss (Figure 7). Though quantifying the relative contributions of these interlinked drivers remains challenging, it is critical to clarify that these factors such as erosion, aridity, winds, and vegetation, function as internal feedback processes rather than independent forcing factors. This lack of clear quantification of the hierarchical roles of these drivers limits predictive understanding of dust cycles. We thus prioritize the development of Earth system models capable of isolating these factors through targeted sensitivity experiments. Under future warming, rapid glacier retreat across the TP and surrounding mountains, along with increased precipitation and vegetation cover in source regions, would reduce the supply of erodible sediments and stabilize surfaces, thereby progressively weakening Asian dust emissions and their impacts on downwind marine productivity and biodiversity.

CONCLUSION

This study provides the first high-resolution 2.7-Myr dust flux record from arid Central Asia west of the Pamir, addressing a key spatial gap in the westerlies-dominated mid-latitude Eurasia. Post-MPT (~0.8 Ma), intensified aridification and a shift to 100-kyr climate cycles coincided with peak Asian dust emissions and amplified glacial–interglacial variability. These changes were closely linked to Northern Hemisphere ice volume, with glacial erosion, aridification, vegetation loss, and stronger winds as the primary drivers of enhanced Asian dust activity during cold periods.

REFERENCES

1. Kok J.F., Storelvmo T., Karydis V.A., et al. (2023). Mineral dust aerosol impacts on global climate and climate change. *Nat. Rev. Earth Environ.* **4**:71–86. DOI:10.1038/s43017-022-00379-5
2. Huang J., Minnis P., Chen B., et al. (2008). Long-range transport and vertical structure of Asian dust from CALIPSO and surface measurements during PACDEX. *J. Geophys. Res. Atmos.* **113**:2008JD010620. DOI:10.1029/2008JD010620
3. Sun J. (2002). Provenance of loess material and formation of loess deposits on the Chinese Loess Plateau. *Earth Planet. Sci. Lett.* **203**:845–859. DOI:10.1016/S0012-821X(02)00921-4
4. Uno I., Eguchi K., Yumimoto K., et al. (2009). Asian dust transported one full circuit around the globe. *Nat. Geosci.* **2**:557–560. DOI:10.1038/ngeo583
5. Jickells T.D., An Z.S., Andersen K.K., et al. (2005). Global iron connections between desert dust, ocean biogeochemistry, and climate. *Science* **308**:67–71. DOI:10.1126/science.1105959
6. Maher B.A., Prospero J.M., Mackie D., et al. (2010). Global connections between aeolian dust, climate and ocean biogeochemistry at the present day and at the last glacial maximum. *Earth Sci. Rev.* **99**:61–97. DOI:10.1016/j.earscirev.2009.12.001
7. Shao Y., Wyrwoll K.H., Chappell A., et al. (2011). Dust cycle: An emerging core theme in Earth system science. *Aeolian Res.* **2**:181–204. DOI:10.1016/j.aeolia.2011.02.001
8. Zan J., Maher B.A., Yamazaki T., et al. (2023). Mid-Pleistocene links between Asian dust, Tibetan glaciers, and Pacific iron fertilization. *Proc. Natl. Acad. Sci. USA* **120**:e2304773120. DOI:10.1073/pnas.2304773120
9. Zan J., Maher B.A., Fang X., et al. (2025). Global dust impacts on biogeochemical cycles and climate. *Nat. Rev. Earth Environ.* **6**:789–807. DOI:10.1038/s43017-025-00734-2
10. Yang X. (1999). The grain size of the windborne sediments in the areas of Keriya river (northwestern China) and its paleoenvironmental interpretation. *Quat. Sci.* **19**:373–379. http://www.dsjyj.com.cn/en/article/id/dsjyj_9590
11. Sun Y. (2020). Source-to-sink fluctuations of Asian aeolian deposits since the late Oligocene. *Earth Sci. Rev.* **200**:102963. DOI:10.1016/j.earscirev.2019.102963
12. Lu H., Wang X., Wang X., et al. (2019). Formation and evolution of Gobi Desert in central and eastern Asia. *Earth Sci. Rev.* **194**:251–263. DOI:10.1016/j.earscirev.2019.04.014
13. Guo Z.T., Ruddiman W.F., Hao Q.Z., et al. (2002). Onset of Asian desertification by 22 Myr ago inferred from loess deposits in China. *Nature* **416**:159–163. DOI:10.1038/416159a
14. Fang X., An Z., Clemens S.C., et al. (2020). The 3.6-Ma aridity and westerlies history over midlatitude Asia linked with global climatic cooling. *Proc. Natl. Acad. Sci. USA* **117**:24729–24734. DOI:10.1073/pnas.1922710117
15. Ding Z.L., Derbyshire E., Yang S.L., et al. (2005). Stepwise expansion of desert environment across northern China in the past 3.5 Ma and implications for monsoon evolution. *Earth Planet. Sci. Lett.* **237**:45–55. DOI:10.1016/j.epsl.2005.06.036
16. Porter S.C. and An Z. (1995). Correlation between climate events in the North Atlantic and China during the last glaciation. *Nature* **375**:305–308. DOI:10.1038/375305a0
17. Han Y., An Z., Marlon J.R., et al. (2020). Asian inland wildfires driven by glacial–interglacial climate change. *Proc. Natl. Acad. Sci. USA* **117**:5184–5189. DOI:10.1073/pnas.1822035117
18. Sun Y. and An Z. (2002). History and variability of Asian interior aridity recorded by eolian flux in the Chinese Loess Plateau during the past 7 Ma. *Sci. China Earth Sci.* **45**:420–429. DOI:10.1360/02yd9044
19. Sun Y. and An Z. (2005). Late Pliocene-Pleistocene changes in mass accumulation rates of eolian deposits on the central Chinese Loess Plateau. *J. Geophys. Res. Atmos.* **110**:2005JD006064. DOI:10.1029/2005JD006064
20. Li B., Sun D., Xu W., et al. (2017). Paleomagnetic chronology and paleoenvironmental records from drill cores from the Hetao Basin and their implications for the formation of the Hobq Desert and the Yellow River. *Quat. Sci. Rev.* **156**:69–89. DOI:10.1016/j.quascirev.2016.11.023
21. Li Z., Sun D., Chen F., et al. (2014). Chronology and paleoenvironmental records of a drill core in the central Tengger Desert of China. *Quat. Sci. Rev.* **85**:85–98. DOI:10.1016/j.quascirev.2013.12.003
22. Wang F., Sun D., Chen F., et al. (2015). Formation and evolution of the Badain Jaran Desert, North China, as revealed by a drill core from the desert centre and by geological survey. *Palaeogeogr. Palaeoclimatol. Palaeoecol.* **426**:139–158. DOI:10.1016/j.palaeo.2015.03.011
23. Wang X., Yu Z., Luo C., et al. (2024). Spatial heterogeneity in the formation of large deserts in midlatitude Asia revealed by drill core evidence. *Sci. Bull.* **69**:3512–3515. DOI:10.1016/j.scib.2024.09.044
24. Zhao H., Sun Y. and Qiang X. (2022). Mid-Pleistocene formation of modern-like desert landscape in North China. *Catena* **216**:106399. DOI:10.1016/j.catena.2022.106399
25. Wang X., Yu Z., Hu H., et al. (2026). Formation and evolution of sandy deserts in China: A review. *Earth Sci. Rev.* **277**:105459. DOI:10.1016/j.earscirev.2026.105459
26. Zhong Y., Liu Y., Yang H., et al. (2024). Orbital controls on North Pacific dust flux during the Late Quaternary. *Geophys. Res. Lett.* **51**:e2023GL106631. DOI:10.1029/2023GL106631
27. Tang Y., Wan S., Clift P.D., et al. (2022). Northward shift of the Northern Hemisphere westerlies in the Early to Late Miocene and its links to Tibetan uplift. *Geophys. Res. Lett.* **49**:e2022GL099311. DOI:10.1029/2022GL099311
28. Rea D.K., Snoeckx H. and Joseph L.H. (1998). Late Cenozoic eolian deposition in the North Pacific: Asian drying, Tibetan uplift, and cooling of the Northern Hemisphere. *Paleoceanography* **13**:215–224. DOI:10.1029/98PA00123
29. Ding Z.L., Ranov V., Yang S.L., et al. (2002). The loess record in southern Tajikistan and correlation with Chinese loess. *Earth Planet. Sci. Lett.* **200**:387–400. DOI:10.1016/S0012-821X(02)00637-4
30. Forster T. and Heller F. (1994). Loess deposits from the Tajik depression (Central Asia): Magnetic properties and paleoclimate. *Earth Planet. Sci. Lett.* **128**:501–512. DOI:10.1016/0012-821X(94)90166-X
31. Zan J., Ning W., Heller F., et al. (2022). Intensified Northern Hemisphere glaciation

facilitates continuous accumulation of Late Pliocene loess on the western margin of the Pamir. *Geophys. Res. Lett.* **49**:e2022GL099629. DOI:10.1029/2022GL099629
32. Wu C., Lin Z., Liu X., et al. (2021). Description of dust emission parameterization in CAS-ESM2 and its simulation of global dust cycle and East Asian dust events. *J. Adv. Model. Earth Syst.* **13**:e2020MS002456. DOI:10.1029/2020MS002456
33. Muhs D.R. (2007). Loess deposits, origins and properties. Elias S.A. (ed.) Encyclopedia of Quaternary Science (Elsevier), pp:1405–1418. DOI:10.1016/B0-444-52747-8/00158-7
34. Wu H., Lu H., Wang J., et al. (2022). A new estimate of global desert area and quantity of dust emission. *Chin. Sci. Bull.* **67**:860–871. DOI:10.1360/TB-2021-1215
35. Yang S. and Ding Z. (2010). Drastic climatic shift at ~2.8 Ma as recorded in eolian deposits of China and its implications for redefining the Pliocene-Pleistocene boundary. *Quat. Int.* **219**:37–44. DOI:10.1016/j.quaint.2009.10.029
36. Westerhold T., Marwan N., Drury A.J., et al. (2020). An astronomically dated record of Earth's climate and its predictability over the last 66 million years. *Science* **369**:1383–1387. DOI:10.1126/science.aba6853
37. Kohfeld K.E. and Harrison S.P. (2001). DIRTMAP: The geological record of dust. *Earth Sci. Rev.* **54**:81–114. DOI:10.1016/S0012-8252(01)00042-3
38. Kohfeld K. (2003). Glacial-interglacial changes in dust deposition on the Chinese Loess Plateau. *Quat. Sci. Rev.* **22**:1859–1878. DOI:10.1016/S0277-3791(03)00166-5
39. Pye K. (1987). Aeolian dust and dust deposits (Academic Press). DOI:10.1016/C2013-0-05007-4
40. Kukla G., Heller F., Ming L.X., et al. (1988). Pleistocene climates in China dated by magnetic susceptibility. *Geology* **16**:811–814. DOI:10.1130/0091-7613(1988)016<0811:PCICDB>2.3.CO;2
41. Janecek T.R. (1985). Eolian sedimentation in the Northwest Pacific Ocean: A preliminary examination of the data from Deep Sea Drilling Project sites 576 and 578. Initial reports of the Deep Sea Drilling Project (U.S. Government Printing Office), pp:399–417. DOI:10.2973/dsdp.proc.86.1985
42. Rea D.K. and Janecek T.R. (1982). Late Cenozoic changes in atmospheric circulation deduced from North Pacific eolian sediments. *Mar. Geol.* **49**:149–167. DOI:10.1016/0025-3227(82)90034-2
43. Lee A.M.F., Maruyama A., Lu S., et al. (2022). Quantification of Asian dust source variabilities in silt and clay fractions since 10 Ma by Parallel Factor (PARAFAC) Endmember Modeling at IODP site U1425 in the Japan Sea. *Lithosphere* **2022**:6818103. DOI:10.2113/2022/6818103
44. Rea D.K. (1994). The paleoclimatic record provided by eolian deposition in the deep sea: The geologic history of wind. *Rev. Geophys.* **32**:159–195. DOI:10.1029/93RG03257
45. Gylesjö S. (2005). Data report: Late Pleistocene terrigenous input to Shatsky Rise, Site 1208. Bralower T.J., Premoli Silva I. and Malone M.J. (eds). Proceedings of the Ocean Drilling Program, Scientific Results, pp:1–7. https://www-odp.tamu.edu/publications//198_SR/VOLUME/CHAPTERS/105.PDF
46. Abell J.T., Winckler G., Anderson R.F., et al. (2021). Poleward and weakened westerlies during Pliocene warmth. *Nature* **589**:70–75. DOI:10.1038/s41586-020-03062-1
47. Tian S., Sun J., Zhang Z., et al. (2021). Loess deposits in the Tajik Basin, Central Asia: Chronology, provenance and palaeoclimatic implications since the Last Glacial. *Boreas* **50**:147–166. DOI:10.1111/bor.12467
48. Wang X., Carrapa B., Chapman J.B., et al. (2019). Parathethys last gasp in Central Asia and Late Oligocene accelerated uplift of the Pamirs. *Geophys. Res. Lett.* **46**:11773–11781. DOI:10.1029/2019GL084838
49. Lisiecki L.E. and Raymo M.E. (2005). A Pliocene-Pleistocene stack of 57 globally distributed benthic $\delta^{18}O$ records. *Paleoceanography* **20**:PA1003. DOI:10.1029/2004PA001071
50. Ma Z., Zan J., Heller F., et al. (2024). Mineralogical and magnetic variations of periglacial loess in SE Tibet reveal mid-Pleistocene expansion of Tibetan glacial activity. *Quat. Sci. Rev.* **330**:108592. DOI:10.1016/j.quascirev.2024.108592
51. Ning W., Zan J., Heller F., et al. (2023). Magnetic proxy of Eurasian loess revealing enhanced physical erosion since the Mid-Pleistocene Transition. *Geophys. Res. Lett.* **50**:e2023GL104411. DOI:10.1029/2023GL104411
52. Wang S., Zan J., Heller F., et al. (2024). Dynamic coupling between intensified physical erosion and Asian dust activity under Late Cenozoic global cooling. *Geophys. Res. Lett.* **51**:e2024GL110717. DOI:10.1029/2024GL110717
53. Zan J., Fang X., Li X., et al. (2019). Long-term variations in the lithogenic susceptibility of Chinese eolian deposits since the Late Pliocene. *Geophys. Res. Lett.* **46**:726–735. DOI:10.1029/2018GL080726
54. Hu Z., Zan J., Yang Y., et al. (2025). Continental erosion controls the geochemical, mineralogical and weathering trends of central North Pacific sediments. *Glob. Planet. Change* **255**:105051. DOI:10.1016/j.gloplacha.2025.105051
55. Wang X., Carrapa B., Sun Y., et al. (2020). The role of the westerlies and orography in Asian hydroclimate since the late Oligocene. *Geology* **48**:728–732. DOI:10.1130/G47400.1
56. Yang L., Zhang W., Fang X., et al. (2020). Aridification recorded by lithofacies and grain size in a continuous Pliocene-Quaternary lacustrine sediment record in the western Qaidam Basin, NE Tibetan Plateau. *Palaeogeogr. Palaeoclimatol. Palaeoecol.* **556**:109903. DOI:10.1016/j.palaeo.2020.109903
57. Zeng L., Yi S., Zhang W., et al. (2020). Provenance of loess deposits and stepwise expansion of the desert environment in NE China since ~1.2 Ma: Evidence from Nd-Sr isotopic composition and grain-size record. *Glob. Planet. Change* **185**:103087. DOI:10.1016/j.gloplacha.2019.103087
58. Zeng L., Lu H., Yi S., et al. (2016). New magnetostratigraphic and pedostratigraphic investigations of loess deposits in north-east China and their implications for regional environmental change during the Mid-Pleistocene climatic transition. *J. Quat. Sci.* **31**:20–32. DOI:10.1002/jqs.2829
59. Fang X. (2002). Loess in the Tian Shan and its implications for the development of the Gurbantunggut Desert and drying of northern Xinjiang. *Chin. Sci. Bull.* **47**:1381. DOI:10.1360/02tb9305
60. Serno S., Winckler G., Anderson R.F., et al. (2014). Eolian dust input to the Subarctic North Pacific. *Earth Planet. Sci. Lett.* **387**:252–263. DOI:10.1016/j.epsl.2013.11.008
61. Zhang W., Chen J., Ji J., et al. (2016). Evolving flux of Asian dust in the North Pacific Ocean since the late Oligocene. *Aeolian Res.* **23**:11–20. DOI:10.1016/j.aeolia.2016.09.004
62. Zhong Y., Shi X., Yang H., et al. (2022). Humidification of Central Asia and equatorward shifts of westerly winds since the late Pliocene. *Commun. Earth Environ.* **3**:274. DOI:10.1038/s43247-022-00604-5
63. Smalley I.J. (1966). The properties of glacial loess and the formation of loess deposits. *SEPM J. Sediment. Res.* **36**:669–676. DOI:10.1306/74D7153C-2B21-11D7-8648000102C1865D
64. Youn J.H., Seong Y.B., Choi J.H., et al. (2014). Loess deposits in the northern Kyrgyz Tien Shan: Implications for the paleoclimate reconstruction during the Late Quaternary. *Catena* **117**:81–93. DOI:10.1016/j.catena.2013.09.007
65. Wright J.S. (2001). "Desert" loess versus "glacial" loess: Quartz silt formation, source areas and sediment pathways in the formation of loess deposits. *Geomorphology* **36**:231–256. DOI:10.1016/S0169-555X(00)00060-X
66. Smalley I., O'Hara-Dhand K., Wint J., et al. (2009). Rivers and loess: The significance of long river transportation in the complex event-sequence approach to loess deposit formation. *Quat. Int.* **198**:7–18. DOI:10.1016/j.quaint.2008.06.009
67. Hodell D.A., Channell J.E.T., Curtis J.H., et al. (2008). Onset of "Hudson Strait" Heinrich events in the eastern North Atlantic at the end of the middle Pleistocene transition (~640 ka). *Paleoceanography* **23**:2008PA001591. DOI:10.1029/2008PA001591
68. Bintanja R. and Van De Wal R.S.W. (2008). North American ice-sheet dynamics and the onset of 100,000-year glacial cycles. *Nature* **454**:869–872. DOI:10.1038/nature07158
69. Balco G. and Rovey C.W. (2010). Absolute chronology for major Pleistocene advances of the Laurentide Ice Sheet. *Geology* **38**:795–798. DOI:10.1130/G30946.1
70. Knutz P.C., Newton A.M.W., Hopper J.R., et al. (2019). Eleven phases of Greenland Ice Sheet shelf-edge advance over the past 2.7 million years. *Nat. Geosci.* **12**:361–368. DOI:10.1038/s41561-019-0340-8
71. Mangerud J., Jansen E. and Landvik J.Y. (1996). Late Cenozoic history of the Scandinavian and Barents Sea ice sheets. *Glob. Planet. Change* **12**:11–26. DOI:10.1016/0921-8181(95)00009-7
72. Knies J., Matthiessen J., Vogt C., et al. (2009). The Plio-Pleistocene glaciation of the Barents Sea–Svalbard region: A new model based on revised chronostratigraphy. *Quat. Sci. Rev.* **28**:812–829. DOI:10.1016/j.quascirev.2008.12.002
73. Böse M., Lüthgens C., Lee J.R., et al. (2012). Quaternary glaciations of northern Europe. *Quat. Sci. Rev.* **44**:1–25. DOI:10.1016/j.quascirev.2012.04.017
74. Lien Ø.F., Hjelstuen B.O., Zhang X., et al. (2022). Late Plio-Pleistocene evolution of the Eurasian Ice Sheets inferred from sediment input along the northeastern Atlantic continental margin. *Quat. Sci. Rev.* **282**:107433. DOI:10.1016/j.quascirev.2022.107433
75. Jansen E., Fronval T., Rack F., et al. (2000). Pliocene-Pleistocene ice rafting history and cyclicity in the Nordic Seas during the last 3.5 Myr. *Paleoceanography* **15**:709–721. DOI:10.1029/1999PA000435
76. Marković S.B., Fitzsimmons K.E., Sprafke T., et al. (2016). The history of Danube loess research. *Quat. Int.* **399**:86–99. DOI:10.1016/j.quaint.2015.09.071
77. Nie J., Pullen A., Garzione C.N., et al. (2018). Pre-Quaternary decoupling between Asian aridification and high dust accumulation rates. *Sci. Adv.* **4**:eaao6977. DOI:10.1126/sciadv.aao6977
78. Nie J., Stevens T., Rittner M., et al. (2015). Loess Plateau storage of Northeastern Tibetan Plateau-derived Yellow River sediment. *Nat. Commun.* **6**:8511. DOI:10.1038/ncomms9511
79. Stevens T., Carter A., Watson T.P., et al. (2013). Genetic linkage between the Yellow River, the Mu Us desert and the Chinese Loess Plateau. *Quat. Sci. Rev.* **78**:355–368. DOI:10.1016/j.quascirev.2012.11.032
80. Herman F., Seward D., Valla P.G., et al. (2013). Worldwide acceleration of mountain erosion under a cooling climate. *Nature* **504**:423–426. DOI:10.1038/nature12877
81. Zhang P., Molnar P. and Downs W.R. (2001). Increased sedimentation rates and grain sizes 2-4 Myr ago due to the influence of climate change on erosion rates. *Nature* **410**:891–897. DOI:10.1038/35073504
82. Molnar P. and England P. (1990). Late Cenozoic uplift of mountain ranges and global climate change: chicken or egg? *Nature* **346**:29–34. DOI:10.1038/346029a0
83. Liu W., Liu Z., Sun J., et al. (2020). Onset of permanent Taklimakan Desert linked to the mid-Pleistocene transition. *Geology* **48**:782–786. DOI:10.1130/G47406.1
84. Zan J., Louys J., Dennell R., et al. (2024). Mid-Pleistocene aridity and landscape

shifts promoted Palearctic hominin dispersals. *Nat. Commun.* **15**:10279. DOI:10.1038/s41467-024-54767-0
85. Wang P., Hu G., Wang H., et al. (2024). Onset of Mid-Pleistocene glaciation in the Eastern Himalayan syntaxis. *Commun. Earth Environ.* **5**:346. DOI:10.1038/s43247-024-01517-1
86. Zhou S., Li J., Zhao J., et al. (2011). Quaternary Glaciations. Ehlers J. and Gibbard P.L. (eds). Developments in Quaternary Sciences (Elsevier), pp:981–1002. DOI:10.1016/B978-0-444-53447-7.00070-2
87. Zhou S., Xie J., Ou X., et al. (2021). Evidence for glaciation predating MIS-6 in the eastern Nyainqêntanglha Range, southeastern Tibet. *Sci. China Earth Sci.* **64**:559–570. DOI:10.1007/s11430-020-9711-2
88. Heyman J. (2014). Paleoglaciation of the Tibetan Plateau and surrounding mountains based on exposure ages and ELA depression estimates. *Quat. Sci. Rev.* **91**:30–41. DOI:10.1016/j.quascirev.2014.03.018
89. Chen Y., Li Y., Zhang M., et al. (2018). Much late onset of Quaternary glaciations on the Tibetan Plateau: Determining the age of the Shishapangma Glaciation using cosmogenic ^{26}Al and ^{10}Be dating. *Sci. Bull.* **63**:306–313. DOI:10.1016/j.scib.2018.01.020
90. Yan Q., Owen L.A., Wei T., et al. (2025). Regime shift to extensive valley glaciations over High Mountain Asia during the Early-Middle Pleistocene. *Nat. Commun.* **16**:5185. DOI:10.1038/s41467-025-60438-5
91. Lawrence K.T., Sosdian S., White H.E., et al. (2010). North Atlantic climate evolution through the Plio-Pleistocene climate transitions. *Earth Planet. Sci. Lett.* **300**:329–342. DOI:10.1016/j.epsl.2010.10.013
92. Ao H., Ruan J., Martinón-Torres M., et al. (2024). Concurrent Asian monsoon strengthening and early modern human dispersal to East Asia during the last interglacial. *Proc. Natl. Acad. Sci. USA* **121**:e2308994121. DOI:10.1073/pnas.2308994121
93. Yuan B., Cui J., Zhu R., et al. (1996). The age, subdivision and correlation of Nihewan Group. *Sci. China Earth Sci.* **26**:67–73. DOI:10.1360/zd1996-26-1-67
94. Li J., Li X., Fan B., et al. (2021). Characteristics of environmental changes during the Mid-Pleistocene transition period in the Changzhi Basin, Shanxi Province. *Acta Geol. Sin.* **95**:3532–3543. DOI:10.19762/j.cnki.dizhixuebao.2021196
95. Wu F., Fang X., Ma Y., et al. (2007). Plio–Quaternary stepwise drying of Asia: Evidence from a 3-Ma pollen record from the Chinese Loess Plateau. *Earth Planet. Sci. Lett.* **257**:160–169. DOI:10.1016/j.epsl.2007.02.029
96. Shen H., Zhao K., Ge J., et al. (2021). Early and Middle Pleistocene vegetation and its impact on faunal succession on the Liaodong Peninsula, Northeast China. *Quat. Int.* **591**:15–23. DOI:10.1016/j.quaint.2020.11.034
97. Cai M., Fang X., Wu F., et al. (2012). Pliocene–Pleistocene stepwise drying of Central Asia: Evidence from paleomagnetism and sporopollen record of the deep borehole SG-3 in the western Qaidam Basin, NE Tibetan Plateau. *Glob. Planet. Change* **94–95**:72–81. DOI:10.1016/j.gloplacha.2012.07.002
98. Cai M., Xu D., Wei M., et al. (2015). Vegetation and climate change in the Beijing plain during the last million years and implications for Homo erectus occupation in North China. *Palaeogeogr. Palaeoclimatol. Palaeoecol.* **432**:29–35. DOI:10.1016/j.palaeo.2015.05.001
99. Zhao Y., Tzedakis P.C., Li Q., et al. (2020). Evolution of vegetation and climate variability on the Tibetan Plateau over the past 1.74 million years. *Sci. Adv.* **6**:eaay6193. DOI:10.1126/sciadv.aay6193
100. Zhou X., Yang J., Wang S., et al. (2018). Vegetation change and evolutionary response of large mammal fauna during the Mid-Pleistocene Transition in temperate northern East Asia. *Palaeogeogr. Palaeoclimatol. Palaeoecol.* **505**:287–294. DOI:10.1016/j.palaeo.2018.06.007
101. Li J., Fang X., Song C., et al. (2014). Late Miocene–Quaternary rapid stepwise uplift of the NE Tibetan Plateau and its effects on climatic and environmental changes. *Quat. Res.* **81**:400–423. DOI:10.1016/j.yqres.2014.01.002
102. De Boer B., Lourens L.J. and Van De Wal R.S.W. (2014). Persistent 400,000-year variability of Antarctic ice volume and the carbon cycle is revealed throughout the Plio-Pleistocene. *Nat. Commun.* **5**:2999. DOI:10.1038/ncomms3999
103. Clark P.U., Shakun J.D., Rosenthal Y., et al. (2024). Global and regional temperature change over the past 4.5 million years. *Science* **383**:884–890. DOI:10.1126/science.adi1908

FUNDING AND ACKNOWLEDGMENTS

The authors thank the Young Scientists Fund (Category A) of the National Natural Science Foundation of China (42525207), the National Natural Science Foundation of China (42525204), the National Key Research and Development Program of China (2023YFF0804500) and the Postdoctoral Fellowship Program of CPSF (GZC20250271) for financial support. The funders had no role in study design, data collection and analysis, decision to publish, or preparation of the manuscript. The authors also thank Drs. Chong Guan, Chihao Chen, Jian Kang, and Yudong Liu for their assistance in the laboratory and in the field.

AUTHOR CONTRIBUTIONS

J.B.Z. and W.X.N. framed the research questions and designed the study; W.X.N., J.B.Z., C.Z., Y.G.Z., and Z.H. inspected the method and analyzed the data; W.X.N. wrote the manuscript with the assistance of J.B.Z., C.Z., W.L.Z., X.M.F, Y.G.Z., and Z.H. All authors contributed to the manuscript and approved the final version.

DECLARATION OF INTERESTS

The authors declare no competing interests.

DATA AND CODE AVAILABILITY

Tajikistan loess dust flux can be obtained from https://doi.org/10.6084/m9.figshare.30647477. Dust fluxes of other terrestrial loess and marine sediments are cited from the literature.[14,17,19,27,28,41–46] Lithogenic susceptibility of Tajikistan loess, Fe^{2+}, and chlorite contents of Tarim Basin loess are derived from the literature.[8,51,54]

SUPPLEMENTAL INFORMATION

It can be found online at https://doi.org/10.59717/j.xinn-geo.2026.100239.